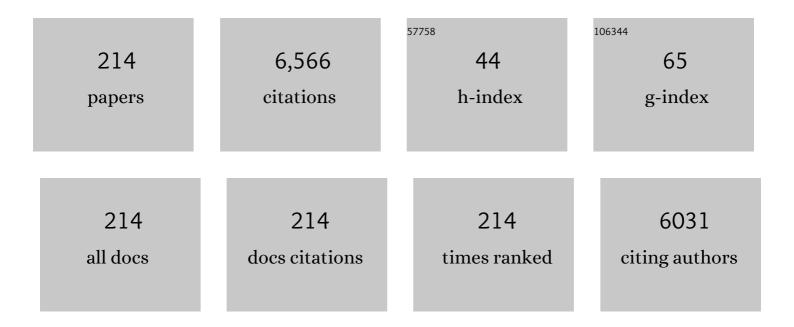
List of Publications by Year in descending order

Source: https://exaly.com/author-pdf/3812690/publications.pdf Version: 2024-02-01



#	Article	IF	CITATIONS
1	Alumina-supported iron oxide nanoparticles as Fischer–Tropsch catalysts: Effect of particle size of iron oxide. Journal of Molecular Catalysis A, 2010, 323, 84-90.	4.8	188
2	Recent progress for direct synthesis of dimethyl ether from syngas on the heterogeneous bifunctional hybrid catalysts. Applied Catalysis B: Environmental, 2017, 217, 494-522.	20.2	181
3	Fischer–Tropsch Synthesis by Carbon Dioxide Hydrogenation on Fe-Based Catalysts. Catalysis Surveys From Asia, 2008, 12, 170-183.	2.6	177
4	Modeling of the Kinetics for Methanol Synthesis using Cu/ZnO/Al <sub>2</sub> O <sub>3</sub> /ZrO <sub>2</sub> Catalyst: Influence of Carbon Dioxide during Hydrogenation. Industrial & Engineering Chemistry Research, 2009, 48, 10448-10455.	3.7	165
5	Facile Synthesis of Hierarchically Structured Bi <sub>2</sub> S <sub>3</sub> /Bi <sub>2</sub> WO <sub>6</sub> Photocatalysts for Highly Efficient Reduction of Cr(VI). ACS Sustainable Chemistry and Engineering, 2015, 3, 2847-2855.	6.7	146
6	Synthesis Strategies, Catalytic Applications, and Performance Regulation of Singleâ€Atom Catalysts. Advanced Functional Materials, 2021, 31, 2008318.	14.9	133
7	Synthesis of nano-sized porous Î <sup>3</sup> -alumina powder via a precipitation/digestion route. Applied Catalysis A: General, 2007, 321, 109-116.	4.3	130
8	Synthesis and characterization of a highly active alumina catalyst for methanol dehydration to dimethyl ether. Applied Catalysis A: General, 2008, 348, 113-120.	4.3	129
9	Recent Advances in Direct Synthesis of Valueâ€Added Aromatic Chemicals from Syngas by Cascade Reactions over Bifunctional Catalysts. Advanced Materials, 2019, 31, e1803390.	21.0	106
10	Single-step synthesis of DME from syngas on Cu–ZnO–Al2O3/zeolite bifunctional catalysts: The superiority of ferrierite over the other zeolites. Fuel Processing Technology, 2008, 89, 1281-1286.	7.2	103
11	Enhanced Stability of Spatially Confined Copper Nanoparticles in an Ordered Mesoporous Alumina for Dimethyl Ether Synthesis from Syngas. ACS Catalysis, 2016, 6, 5629-5640.	11.2	101
12	Microtopographyâ€Guided Conductive Patterns of Liquidâ€Driven Graphene Nanoplatelet Networks for Stretchable and Skinâ€Conformal Sensor Array. Advanced Materials, 2017, 29, 1606453.	21.0	101
13	Synthesis of DME from syngas on the bifunctional Cu–ZnO–Al2O3/Zr-modified ferrierite: Effect of Zr content. Applied Catalysis B: Environmental, 2009, 90, 426-435.	20.2	95
14	Key properties of Ni–MgO–CeO <sub>2</sub> , Ni–MgO–ZrO <sub>2</sub> , and Ni–MgO–Ce <sub>(1â°`x)</sub> Zr <sub>(x)</sub> O <sub>2</sub> catalysts for the reforming of methane with carbon dioxide. Green Chemistry, 2018, 20, 1621-1633.	9.0	90
15	Dimethyl ether synthesis from syngas over the composite catalysts of Cu–ZnO–Al2O3/Zr-modified zeolites. Catalysis Communications, 2008, 9, 2035-2039.	3.3	78
16	Novel aluminophosphate (AlPO) bound ZSM-5 extrudates with improved catalytic properties for methanol to propylene (MTP) reaction. Applied Catalysis A: General, 2010, 374, 18-25.	4.3	73
17	Coproduction of Methanol and Dimethyl Ether from Biomass-Derived Syngas on a Cuâ^'ZnOâ^'Al <sub>2</sub> O <sub>3</sub> /γ-Al <sub>2</sub> O <sub>3</sub> Hybrid Catalyst. Energy & Fuels, 2008, 22, 223-230.	5.1	72
18	Fischer–Tropsch Synthesis Using Zeolite-supported Iron Catalysts for the Production of Light Hydrocarbons. Catalysis Letters, 2008, 125, 264-270.	2.6	71

#	Article	IF	CITATIONS
19	ZSM-5 supported iron catalysts for Fischer–Tropsch production of light olefin. Fuel Processing Technology, 2010, 91, 399-403.	7.2	64
20	Roles of Structural Promoters for Direct CO <sub>2</sub> Hydrogenation to Dimethyl Ether over Ordered Mesoporous Bifunctional Cu/M–Al <sub>2</sub> O <sub>3</sub> (M = Ga or Zn). ACS Catalysis, 2019, 9, 679-690.	11.2	64
21	Highly Ordered Mesoporous Fe <sub>2</sub> O <sub>3</sub> –ZrO <sub>2</sub> Bimetal Oxides for an Enhanced CO Hydrogenation Activity to Hydrocarbons with Their Structural Stability. ACS Catalysis, 2017, 7, 5955-5964.	11.2	63
22	Ga-doped Cu/H-nanozeolite-Y catalyst for selective hydrogenation and hydrodeoxygenation of lignin-derived chemicals. Green Chemistry, 2018, 20, 3253-3270.	9.0	60
23	Catalytic performance on iron-based Fischer–Tropsch catalyst in fixed-bed and bubbling fluidized-bed reactor. Applied Catalysis B: Environmental, 2011, 103, 169-180.	20.2	59
24	Review of Acetic Acid Synthesis from Various Feedstocks Through Different Catalytic Processes. Catalysis Surveys From Asia, 2016, 20, 173-193.	2.6	58
25	Stabilized ordered-mesoporous Co3O4 structures using Al pillar for the superior CO hydrogenation activity to hydrocarbons. Applied Catalysis B: Environmental, 2016, 180, 139-149.	20.2	57
26	Effect of support and cobalt precursors on the activity of Co/AlPO4 catalysts in Fischer–Tropsch synthesis. Journal of Molecular Catalysis A, 2009, 311, 7-16.	4.8	56
27	ZSM-5 Supported Cobalt Catalyst for the Direct Production of Gasoline Range Hydrocarbons by Fischer–Tropsch Synthesis. Catalysis Letters, 2011, 141, 1464-1471.	2.6	56
28	Effect of copper surface area and acidic sites to intrinsic catalytic activity for dimethyl ether synthesis from biomass-derived syngas. Applied Catalysis B: Environmental, 2012, 126, 1-8.	20.2	56
29	Slurry-Phase Fischer–Tropsch Synthesis Using Co/γ-Al2O3, Co/SiO2 and Co/TiO2: Effect of Support on Catalyst Aggregation. Catalysis Letters, 2009, 130, 403-409.	2.6	55
30	Phosphorus induced hydrothermal stability and enhanced catalytic activity of ZSM-5 in methanol to DME conversion. Fuel, 2009, 88, 1915-1921.	6.4	55
31	Efficient Utilization of Greenhouse Gas in a Gas-to-Liquids Process Combined with Carbon Dioxide Reforming of Methane. Environmental Science & Technology, 2010, 44, 1412-1417.	10.0	55
32	Combined Steam and Carbon Dioxide Reforming of Methane on Ni/MgAl2O4: Effect of CeO2 Promoter to Catalytic Performance. Catalysis Letters, 2011, 141, 224-234.	2.6	55
33	Reduction and oxidation kinetics of different phases of iron oxides. International Journal of Hydrogen Energy, 2015, 40, 2613-2620.	7.1	55
34	Aqueous Phase Synthesis of 5-Hydroxymethylfurfural from Glucose over Large Pore Mesoporous Zirconium Phosphates: Effect of Calcination Temperature. ACS Omega, 2018, 3, 808-820.	3.5	54
35	Effect of alkali and alkaline earth metal on Co/CeO 2 catalyst for the water-gas shift reaction of waste derived synthesis gas. Applied Catalysis A: General, 2018, 551, 63-70.	4.3	51
36	Effect of precipitants during the preparation of Cu-ZnO-Al2O3/Zr-ferrierite catalyst on the DME synthesis from syngas. Journal of Industrial and Engineering Chemistry, 2009, 15, 566-572.	5.8	50

#	Article	IF	CITATIONS
37	Catalyst deactivation by carbon formation during CO hydrogenation to hydrocarbons on mesoporous Co3O4. Microporous and Mesoporous Materials, 2014, 188, 196-202.	4.4	50
38	Selective carbonylation of dimethyl ether to methyl acetate on Ferrierite. Catalysis Communications, 2016, 75, 28-31.	3.3	50
39	Hydrodechlorination of CCl4 over Pt/Al2O3: effects of platinum particle size on product distribution. Applied Catalysis A: General, 2003, 240, 129-142.	4.3	49
40	Roles of Ruthenium–Support Interactions of Size-Controlled Ruthenium Nanoparticles for the Product Distribution of Fischer–Tropsch Synthesis. ACS Catalysis, 2014, 4, 1054-1060.	11.2	49
41	Metal oxide (MgO, CaO, and La2O3) promoted Ni-CeO.8ZrO.2O2 catalysts for H2 and CO production from two major greenhouse gases. Renewable Energy, 2015, 79, 91-95.	8.9	47
42	Enhanced Fischer–Tropsch activity on Co/P–Al2O3 catalyst: Effect of phosphorous content. Catalysis Communications, 2009, 10, 1358-1362.	3.3	46
43	Enhanced Catalytic Performance for Dimethyl Ether Synthesis from Syngas with the Addition of Zr or Ga on a Cuâ^'ZnOâ^'Al2O3/γ-Al2O3 Bifunctional Catalyst. Energy & Fuels, 2010, 24, 804-810.	5.1	46
44	Synthesis and characterization of Pt-, Pd-, and Ru-promoted Ni–Ce0.6Zr0.4O2 catalysts for efficient biodiesel production by deoxygenation of oleic acid. Fuel, 2019, 236, 928-933.	6.4	45
45	Effect of CO2 in the feed stream on the deactivation of Co/γ-Al2O3 Fischer–Tropsch catalyst. Catalysis Communications, 2008, 9, 2269-2273.	3.3	44
46	Crucial factors for catalyst aggregation and deactivation on Co/Al2O3 in a slurry-phase Fischer–Tropsch synthesis. Applied Catalysis A: General, 2012, 413-414, 310-321.	4.3	44
47	Highly stable and selective layered Co-Al-O catalysts for low-temperature CO2 methanation. Applied Catalysis B: Environmental, 2022, 310, 121303.	20.2	43
48	Ru promoted cobalt catalyst on γ-Al2O3 support: Influence of pre-synthesized nanoparticles on Fischer–Tropsch reaction. Journal of Molecular Catalysis A, 2011, 344, 153-160.	4.8	42
49	New reaction pathways and kinetic parameter estimation for methanol dehydration over modified ZSM-5 catalysts. Applied Catalysis A: General, 2011, 395, 95-106.	4.3	42
50	Ni/M-Al2O3 (M=Sm, Ce or Mg) for combined steam and CO2 reforming of CH4 from coke oven gas. Journal of CO2 Utilization, 2017, 21, 211-218.	6.8	42
51	Influence of Ru segregation on the activity of Ru–Co/γ-Al2O3 during FT synthesis: A comparison with that of Ru–Co/SiO2 catalysts. Catalysis Communications, 2008, 9, 2282-2286.	3.3	39
52	Enhanced Catalytic Performance by Zirconium Phosphateâ€Modified SiO <sub>2</sub> â€&upported RuCo Catalyst for Fischer–Tropsch Synthesis. ChemCatChem, 2011, 3, 1342-1347.	3.7	39
53	Non-stoichiometric SnS microspheres with highly enhanced photoreduction efficiency for Cr( <scp>vi</scp> ) ions. RSC Advances, 2017, 7, 30533-30541.	3.6	38
54	Influence of pH of the Impregnation Solution on the Catalytic Properties of Co/γ-Alumina for Fischerâ^²Tropsch Synthesis. Energy & Fuels, 2008, 22, 2885-2891.	5.1	37

JONG-WOOK BAE

#	Article	IF	CITATIONS
55	Development of a kinetic model of the Fischer–Tropsch synthesis reaction with a cobalt-based catalyst. Reaction Kinetics, Mechanisms and Catalysis, 2011, 104, 483-502.	1.7	36
56	Faradaic reaction of dual-redox additive in zwitterionic gel electrolyte boosts the performance of flexible supercapacitors. Electrochimica Acta, 2019, 319, 672-681.	5.2	36
57	Influence of bimodal pore size distribution of Ru/Co/ZrO2–Al2O3 during Fischer–Tropsch synthesis in fixed-bed and slurry reactor. Journal of Molecular Catalysis A, 2009, 298, 81-87.	4.8	35
58	Gas-Phase Carbonylation of Dimethyl Ether on the Stable Seed-Derived Ferrierite. ACS Catalysis, 2020, 10, 5135-5146.	11.2	35
59	Effect of Cu content on the bifunctional Fischer–Tropsch Fe–Cu–K/ZSM5 catalyst. Journal of Industrial and Engineering Chemistry, 2009, 15, 798-802.	5.8	34
60	Combined Steam and CO <sub>2</sub> Reforming of CH <sub>4</sub> on LaSrNiO <sub><i>x</i></sub> Mixed Oxides Supported on Al <sub>2</sub> O <sub>3</sub> -Modified SiC Support. Energy & Fuels, 2015, 29, 1055-1065.	5.1	34
61	Successive reduction-oxidation activity of FeOx/TiO2 for dehydrogenation of ethane and subsequent CO2 activation. Applied Catalysis B: Environmental, 2020, 270, 118887.	20.2	34
62	Direct conversion of synthesis gas to light olefins using dual bed reactor. Journal of Industrial and Engineering Chemistry, 2009, 15, 847-853.	5.8	33
63	Reaction modeling on the phosphorous-treated Ru/Co/Zr/SiO2 Fischer–Tropsch catalyst with the estimation of kinetic parameters and hydrocarbon distribution. Fuel, 2011, 90, 1383-1394.	6.4	33
64	Hydrodechlorination of CCl4 over Pt/ $\hat{l}^3$ -Al2O3. Applied Catalysis A: General, 2001, 217, 79-89.	4.3	32
65	Effect of Preparation Method of Fe–based Fischer–Tropsch Catalyst on their Light Olefin Production. Catalysis Letters, 2009, 130, 630-636.	2.6	32
66	Fischer–Tropsch synthesis on cobalt/Al <sub>2</sub> O <sub>3</sub> -modified SiC catalysts: effect of cobalt–alumina interactions. Catalysis Science and Technology, 2014, 4, 343-351.	4.1	32
67	Fischer–Tropsch synthesis on Co/AlSBA-15: effects of hydrophilicity of supports on cobalt dispersion and product distributions. Catalysis Science and Technology, 2015, 5, 3525-3535.	4.1	32
68	Optimization of Cobalt Loading in Co–CeO2 Catalyst for the High Temperature Water–Gas Shift Reaction. Topics in Catalysis, 2017, 60, 721-726.	2.8	32
69	Adjusted interactions of nickel nanoparticles with cobalt-modified MgAl2O4-SiC for an enhanced catalytic stability during steam reforming of propane. Applied Catalysis A: General, 2018, 549, 117-133.	4.3	32
70	Current Catalyst Technology of Selective Catalytic Reduction (SCR) for NOx Removal in South Korea. Catalysts, 2020, 10, 52.	3.5	32
71	Role of ZSM5 Distribution on Co/SiO <sub>2</sub> Fischer–Tropsch Catalyst for the Production of C <sub>5</sub> –C <sub>22</sub> Hydrocarbons. Energy & Fuels, 2012, 26, 6061-6069.	5.1	31
72	Single-step synthesis of dimethyl ether from syngas on Al2O3-modified CuO–ZnO–Al2O3/ferrierite catalysts: Effects of Al2O3 content. Catalysis Today, 2014, 228, 175-182.	4.4	31

#	Article	IF	CITATIONS
73	Influence of Ga addition on the methanol synthesis activity of Cu/ZnO catalyst in the presence and absence of alumina. Journal of Industrial and Engineering Chemistry, 2009, 15, 665-669.	5.8	30
74	Effect of Copper Precursors to the Activity for Dimethyl Ether Synthesis from Syngas over Cu–ZnO/l³-Al <sub>2</sub> O <sub>3</sub> Bifunctional Catalysts. Energy & Fuels, 2011, 25, 2438-2443.	5.1	30
75	Effects of Carbon Formation on Catalytic Performance for CO <sub>2</sub> Reforming with Methane on Ni/Al <sub>2</sub> O <sub>3</sub> Catalyst: Comparison of Fixed-Bed with Fluidized-Bed Reactors. Industrial & Engineering Chemistry Research, 2013, 52, 13288-13296.	3.7	30
76	Aqueous phase reforming of polyols for hydrogen production using supported Pt Fe bimetallic catalysts. Renewable Energy, 2016, 95, 396-403.	8.9	30
77	Enhanced Production of C2–C4 Olefins Directly from Synthesis Gas. Catalysis Letters, 2008, 126, 149-154.	2.6	29
78	The role of CeO2–ZrO2 distribution on the Ni/MgAl2O4 catalyst during the combined steam and CO2 reforming of methane. Reaction Kinetics, Mechanisms and Catalysis, 2011, 104, 377-388.	1.7	29
79	Water gas shift reaction on the Mn-modified ordered mesoporous Co 3 O 4. Microporous and Mesoporous Materials, 2016, 221, 204-211.	4.4	29
80	Aqueous phase reforming of ethylene glycol over bimetallic platinum-cobalt on ceria–zirconia mixed oxide. International Journal of Hydrogen Energy, 2017, 42, 9892-9902.	7.1	29
81	Gas holdup and hydrodynamic flow regime transition in bubble columns. Journal of Industrial and Engineering Chemistry, 2017, 56, 450-462.	5.8	29
82	Low temperature steam reforming of methane using metal oxide promoted Ni-Ce0.8Zr0.2O2 catalysts in a compact reformer. International Journal of Hydrogen Energy, 2018, 43, 262-270.	7.1	29
83	Dimethyl ether carbonylation to methyl acetate over highly crystalline zeolite seed-derived ferrierite. Catalysis Science and Technology, 2018, 8, 3060-3072.	4.1	29
84	Hydrodechlorination of CCl4 over Pt/γ-Al2O3 prepared from different Pt precursors. Applied Catalysis A: General, 2008, 334, 156-167.	4.3	28
85	Combined steam and CO2 reforming of CH4 using coke oven gas on nickel-based catalyst: Effects of organic acids to nickel dispersion and activity. Chemical Engineering Journal, 2015, 280, 771-781.	12.7	28
86	Fischer–Tropsch synthesis on the Al2O3-modified ordered mesoporous Co3O4 with an enhanced catalytic activity and stability. Catalysis Today, 2016, 265, 27-35.	4.4	28
87	Effects of titanium impurity on alumina surface for the activity of Co/Ti–Al2O3 Fischer–Tropsch catalyst. Applied Catalysis A: General, 2012, 419-420, 148-155.	4.3	26
88	Novel heterogeneous Rh-incorporated graphitic-carbon nitride for liquid-phase carbonylation of methanol to acetic acid. Catalysis Communications, 2017, 99, 141-145.	3.3	26
89	Textural Properties and Catalytic Applications of ZSM-5 Monolith Foam for Methanol Conversion. Catalysis Letters, 2009, 129, 408-415.	2.6	25
90	Performance of a slurry bubble column reactor for Fischer–Tropsch synthesis: Determination of optimum condition. Fuel Processing Technology, 2010, 91, 434-439.	7.2	25

#	Article	IF	CITATIONS
91	Deactivation behaviors of Pt or Ru promoted Co/P-Al2O3 catalysts during slurry-phase Fischer–Tropsch synthesis. Catalysis Communications, 2011, 12, 539-543.	3.3	25
92	Kinetics modeling for the mixed reforming of methane over Ni-CeO2/MgAl2O4 catalyst. Journal of Natural Gas Chemistry, 2011, 20, 9-17.	1.8	25
93	Effects of Cu–ZnO Content on Reaction Rate for Direct Synthesis of DME from Syngas with Bifunctional Cu–ZnO/γ-Al2O3 Catalyst. Catalysis Letters, 2013, 143, 666-672.	2.6	25
94	Deactivation Behavior of Co/SiC Fischer–Tropsch Catalysts by Formation of Filamentous Carbon. Catalysis Letters, 2013, 143, 18-22.	2.6	25
95	Special issue of the 15th Korea–Japan Symposium on Catalysis (15th KJSC). Research on Chemical Intermediates, 2016, 42, 1-2.	2.7	25
96	Unprecedented activity and stability on zirconium phosphates grafted mesoporous silicas for renewable aromatics production from furans. Journal of Catalysis, 2020, 385, 10-20.	6.2	25
97	Noble-Metal-Based Catalytic Oxidation Technology Trends for Volatile Organic Compound (VOC) Removal. Catalysts, 2022, 12, 63.	3.5	25
98	Effect of Al2O3 content on the adsorptive properties of Cu/ZnO/Al2O3 for removal of odorant sulfur compounds. International Journal of Hydrogen Energy, 2009, 34, 8733-8740.	7.1	24
99	Optimization of a highly active nano-sized Pt/CeO2 catalyst via Ce(OH)CO3 for the water-gas shift reaction. Renewable Energy, 2015, 79, 78-84.	8.9	24
100	Ordered mesoporous CoMOx (M = Al or Zr) mixed oxides for Fischer–Tropsch synthesis. Chemical Communications, 2016, 52, 4820-4823.	4.1	24
101	Rh-Mn/tungsten carbides for direct synthesis of mixed alcohols from syngas: Effects of tungsten carbide phases. Microporous and Mesoporous Materials, 2018, 255, 44-52.	4.4	24
102	Effect of calcination temperature on the association between free NiO species and catalytic activity of Niâ^'Ce0.6Zr0.4O2 deoxygenation catalysts for biodiesel production. Renewable Energy, 2019, 131, 144-151.	8.9	24
103	Increase in stability of BaCo/CeO2 catalyst by optimizing the loading amount of Ba promoter for high-temperature water-gas shift reaction using waste-derived synthesis gas. Renewable Energy, 2020, 145, 2715-2722.	8.9	24
104	Effective Removal of Odorants in Gaseous Fuel for the Hydrogen Station Using Hydrodesulfurization and Adsorption. Energy & amp; Fuels, 2007, 21, 3537-3540.	5.1	23
105	Deactivation by Filamentous Carbon Formation on Co/Aluminum Phosphate during Fischerâ^Tropsch Synthesis. Industrial & Engineering Chemistry Research, 2009, 48, 3228-3233.	3.7	22
106	Morphological variation of highly porous Ni–Sn foams fabricated by electro-deposition in hydrogen-bubble templates and their performance as pseudo-capacitors. Applied Surface Science, 2014, 322, 15-20.	6.1	22
107	Capacitance enhancement in supercapacitors by incorporating ultra-long hydrated vanadium-oxide nanobelts into graphene. Journal of Alloys and Compounds, 2016, 688, 814-821.	5.5	22
108	Direct activation of CH4 to oxygenates and unsaturated hydrocarbons using N2O on Fe-modified zeolites. Journal of Molecular Catalysis A, 2017, 426, 130-140.	4.8	22

#	Article	IF	CITATIONS
109	Thermally Stabilized Cobaltâ€Based Fischer–Tropsch Catalysts by Phosphorous Modification of Al <sub>2</sub> O <sub>3</sub> : Effect of Calcination Temperatures on Catalyst Stability. ChemCatChem, 2015, 7, 1460-1469.	3.7	21
110	Highly stable seed-derived ferrierite for carbonylation of dimethyl ether to methyl acetate: Effects of seed content to catalytic stability. Catalysis Today, 2020, 339, 79-85.	4.4	21
111	Sulfur-Tolerant Pt/CeO <sub>2</sub> Catalyst with Enhanced Oxygen Storage Capacity by Controlling the Pt Content for the Waste-to-Hydrogen Processes. ACS Sustainable Chemistry and Engineering, 2021, 9, 15287-15293.	6.7	21
112	Modeling a slurry CSTR with Co/P–Al2O3 catalyst for Fischer–Tropsch synthesis. Fuel Processing Technology, 2011, 92, 2264-2271.	7.2	20
113	Reduction-oxidation kinetics of three different iron oxide phases for CO 2 activation to CO. Fuel, 2017, 202, 547-555.	6.4	20
114	The effect of titration time on the catalytic performance of Cu/CeO 2 catalysts for water-gas shift reaction. Catalysis Today, 2018, 309, 83-88.	4.4	20
115	Synergistic effects of Nb 2 O 5 promoter on Ru/Al 2 O 3 for an aqueous-phase hydrodeoxygenation of glycerol to hydrocarbons. Applied Catalysis A: General, 2018, 551, 49-62.	4.3	20
116	Effect of Active Component Contents to Catalytic Performance on Fe-Cu-K/ZSM5 Fischer-Tropsch Catalysis Letters, 2010, 134, 233-241.	2.6	19
117	Effects of ordered mesoporous bimodal structures of Fe/KIT-6 for CO hydrogenation activity to hydrocarbons. Chemical Engineering Journal, 2018, 354, 197-207.	12.7	19
118	Enhanced thermal stability of Ni nanoparticles in ordered mesoporous supports for dry reforming of methane with CO2. Catalysis Today, 2022, 388-389, 224-230.	4.4	19
119	Effects of Pt precursors on Pt/CeO2 to water-gas shift (WGS) reaction activity with Langmuir-Hinshelwood model-based kinetics. International Journal of Hydrogen Energy, 2020, 45, 26953-26966.	7.1	19
120	Highly active and stable catalytic performance on phosphorous-promoted Ru/Co/Zr/SiO2 Fischer–Tropsch catalyst. Catalysis Communications, 2010, 11, 834-838.	3.3	18
121	Facile synthesis of flower-like α-Co(OH) 2 nanostructures for electrochemical water splitting and pseudocapacitor applications. Journal of Industrial and Engineering Chemistry, 2016, 37, 175-179.	5.8	18
122	Effect of the ordered meso–macroporous structure of Co/SiO <sub>2</sub> on the enhanced activity of hydrocarbons. Catalysis Science and Technology, 2016, 6, 4221-4231.	4.1	18
123	Effects of surface modification with zirconium phosphate on Ru/Co/SiO2 Fischer–Tropsch catalysts analyzed by XPS and TEM analyses. Applied Catalysis A: General, 2013, 450, 88-95.	4.3	17
124	Roles of Al2O3 promoter for an enhanced structural stability of ordered-mesoporous Co3O4 catalyst during CO hydrogenation to hydrocarbons. Fuel, 2018, 225, 460-471.	6.4	17
125	Effects of metal-organic framework-derived iron carbide phases for CO hydrogenation activity to hydrocarbons. Fuel, 2020, 281, 118779.	6.4	17
126	Effect of Calcination Temperature on the Activity and Cobalt Crystallite Size of Fischer–Tropsch Co–Ru–Zr/SiO2 Catalyst. Catalysis Letters, 2009, 129, 233-239.	2.6	16

#	Article	IF	CITATIONS
127	Cyclic production of syngas and hydrogen through methane-reforming and water-splitting by using ceria–zirconia solid solutions in a solar volumetric receiver–reactor. Solar Energy, 2014, 109, 70-81.	6.1	16
128	Spatially confined cobalt nanoparticles on zirconium phosphate-modified KIT-6 for an enhanced stability of CO hydrogenation to hydrocarbons. Fuel, 2019, 239, 547-558.	6.4	16
129	Liquid-phase hydrodechlorination of CCl4 in a medium of ethanol with co-production of acetal and diethyl carbonate. Journal of Molecular Catalysis A, 2003, 206, 225-238.	4.8	15
130	Esterification of acetic acid with methanol to methyl acetate on Pd-modified zeolites: effect of BrÃ,nsted acid site strength on activity. Reaction Kinetics, Mechanisms and Catalysis, 2014, 112, 499-510.	1.7	15
131	Aqueous phase reforming and hydrodeoxygenation of ethylene glycol on Pt/SiO2–Al2O3: effects of surface acidity on product distribution. RSC Advances, 2016, 6, 68433-68444.	3.6	15
132	Synergy effects of basic graphitic-C3N4 over acidic Al2O3 for a liquid-phase decarboxylation of naphthenic acids. Fuel Processing Technology, 2019, 184, 36-44.	7.2	15
133	Optimization of methanol synthesis reaction on Cu/ZnO/Al2O3/ZrO2 catalyst using genetic algorithm: Maximization of the synergetic effect by the optimal CO2 fraction. Korean Journal of Chemical Engineering, 2010, 27, 1760-1767.	2.7	14
134	The investigation of non-noble metal doped mesoporous cobalt oxide catalysts for the water–gas shift reaction. RSC Advances, 2016, 6, 52754-52760.	3.6	14
135	Roles of phosphorous-modified Al2O3 for an enhanced stability of Co/Al2O3 for CO hydrogenation to hydrocarbons. Journal of Molecular Catalysis A, 2017, 426, 177-189.	4.8	14
136	Effects of CO <sub>2</sub> on the deactivation behaviors of Co/Al <sub>2</sub> O <sub>3</sub> and Co/SiO <sub>2</sub> in CO hydrogenation to hydrocarbons. Catalysis Science and Technology, 2017, 7, 4079-4091.	4.1	14
137	Selective ethanol synthesis via multi-step reactions from syngas: Ferrierite-based catalysts and fluidized-bed reactor application. Catalysis Today, 2018, 303, 93-99.	4.4	14
138	Effects of Tin on Product Distribution and Catalyst Stability in Hydrodechlorination of CCl4over Pt-Sn/γ-Al2O3. Industrial & Engineering Chemistry Research, 2007, 46, 1721-1730.	3.7	13
139	Controlled Nanocrystal Deposition for Higher Degree of Reduction in Co/Al2O3 Catalyst. Catalysis Letters, 2009, 130, 198-203.	2.6	13
140	Correlation of the amount of carbonaceous species with catalytic performance on iron-based Fischer–Tropsch catalysts. Fuel Processing Technology, 2013, 109, 141-149.	7.2	13
141	A Fluorescent Tile DNA Diagnocode System for In Situ Rapid and Selective Diagnosis of Cytosolic RNA Cancer Markers. Scientific Reports, 2015, 5, 18497.	3.3	13
142	The role of the acidity of alumina prepared by aluminum-carbon black composite for CO hydrogenation to dimethyl ether on hybrid Cu–ZnO–Al2O3/alumina. Reaction Kinetics, Mechanisms and Catalysis, 2015, 116, 173-189.	1.7	13
143	Fischer-Trospch Synthesis on Ordered Mesoporous Cobalt-Based Catalysts with Compact Multichannel Fixed-Bed Reactor Application: A Review. Catalysis Surveys From Asia, 2016, 20, 210-230.	2.6	13
144	Ordered Mesoporous Co <sub>3</sub> O <sub>4</sub> â^'Al <sub>2</sub> O <sub>3</sub> Binary Metal Oxides for CO Hydrogenation to Hydrocarbons: Synergy Effects of Phosphorus Modifier for an Enhanced Catalytic Activity and Stability. ChemCatChem, 2019, 11, 1707-1721.	3.7	13

JONG-WOOK BAE

#	Article	IF	CITATIONS
145	Crucial factors to maximize DME productivity on hydrophobic bifunctional Cu-ZnO-Al2O3/ferrierite by direct CO2 hydrogenation. Catalysis Today, 2021, 369, 112-122.	4.4	13
146	Effects of spatially confined nickel nanoparticles in surface-pretreated hydrophobic SBA-15 for dry reforming of CH4 with CO2. Journal of CO2 Utilization, 2021, 51, 101629.	6.8	13
147	Morphology Effects of Ferrierite on Bifunctional Cu–ZnO–Al <sub>2</sub> O <sub>3</sub> /Ferrierite for Direct Syngas Conversion to Dimethyl Ether. ACS Catalysis, 2021, 11, 14210-14223.	11.2	13
148	Catalytic Performance and Kinetic Models on Zirconium Phosphate Modified Ru/Co/SiO2 Fischer–Tropsch Catalyst. Catalysis Surveys From Asia, 2012, 16, 121-137.	2.6	12
149	Rapid synthesis of magnetite catalysts incorporated with M (Cu, Ni, Zn, and Co) promoters for high temperature water gas shift reaction. New Journal of Chemistry, 2014, 38, 4872-4878.	2.8	12
150	Kinetic models of Fischer-Tropsch synthesis reaction over granule-type Pt-promoted Co/Al2O3 catalyst. Korean Journal of Chemical Engineering, 2018, 35, 1263-1273.	2.7	12
151	Ethanol conversion into 1,3-butadiene over Zn Zr mixed oxide catalysts supported on ordered mesoporous materials. Fuel Processing Technology, 2020, 200, 106317.	7.2	12
152	Carbonylation of dimethyl ether on ferrierite zeolite: Effects of crystallinity to coke distribution and deactivation. Microporous and Mesoporous Materials, 2021, 310, 110669.	4.4	12
153	Oxidative dehydrogenation of ethane and subsequent CO2 activation on Ce-incorporated FeTiOx metal oxides. Chemical Engineering Journal, 2022, 433, 134621.	12.7	12
154	Aqueous phase reforming of ethylene glycol on Pt/CeO <sub>2</sub> –ZrO <sub>2</sub> : effects of cerium to zirconium molar ratio. RSC Advances, 2015, 5, 54806-54815.	3.6	11
155	Methyl Acetate Synthesis by Esterification on the Modified Ferrierite: Correlation of Acid Sites Measured by Pyridine IR and NH <sub>3</sub> -TPD for Steady-State Activity. Journal of Nanoscience and Nanotechnology, 2016, 16, 4626-4630.	0.9	11
156	Hydrodynamic characteristics at the layer inversion point in three-phase fluidized beds with binary solids. Chemical Engineering Science, 2017, 157, 99-106.	3.8	11
157	Synergy Effects of Cobalt Oxides on Ni/Co-Embedded Al2O3 for Hydrogen-Rich Syngas Production by Steam Reforming of Propane. Catalysts, 2020, 10, 461.	3.5	11
158	Phosphorusâ€Modified Mesoporous Inorganic Materials for Production of Hydrocarbon Fuels and Valueâ€Added Chemicals. ChemCatChem, 2020, 12, 4224-4241.	3.7	11
159	Roles of highly ordered mesoporous structures of Fe–Ni bimetal oxides for an enhanced high-temperature water-gas shift reaction activity. Catalysis Science and Technology, 2021, 11, 3251-3260.	4.1	11
160	Unprecedented contributions of In2O3 promoter on ordered mesoporous Cu/Al2O3 for CO2 hydrogenation to oxygenates. Chemical Engineering Journal, 2022, 439, 135649.	12.7	11
161	Solid mass flux in a chemical-looping process for hydrogen production in a multistage circulating moving bed reactor. International Journal of Hydrogen Energy, 2013, 38, 6052-6058.	7.1	10
162	Effects of phosphorus and saccharide on size, shape, and reducibility of Fischer–Tropsch catalysts for slurry phase and fixed-bed reactions. Applied Catalysis A: General, 2013, 453, 358-369.	4.3	10

#	Article	IF	CITATIONS
163	Fischer-Tropsch synthesis on the cobalt impregnated catalyst using carbon-coated Ni/SiO2. Korean Journal of Chemical Engineering, 2016, 33, 1565-1570.	2.7	10
164	Fischer–Tropsch synthesis on potassium-modified Fe3O4 nanoparticles. Research on Chemical Intermediates, 2016, 42, 335-350.	2.7	10
165	Synergy effects of Al2O3 promoter on a highly ordered mesoporous heterogeneous Rh-g-C3N4 for a liquid-phase carbonylation of methanol. Applied Catalysis A: General, 2019, 585, 117209.	4.3	10
166	Effect of Phosphorus Modification on Cuâ^'ZnOâ^'Al2O3for the Removal of H2S. Energy & Fuels, 2008, 22, 2580-2584.	5.1	9
167	Catalytic performance on CuO–Cr2O3–Ga2O3 mixed oxides for water gas shift reaction: Effects of Ga/Cr molar ratio. Catalysis Communications, 2012, 19, 66-69.	3.3	9
168	Preferential CO oxidation over supported Pt catalysts. Korean Journal of Chemical Engineering, 2016, 33, 1781-1787.	2.7	9
169	Direct Conversion of CO2 into Dimethyl Ether over Al2O3/Cu/ZnO Catalysts Prepared by Sequential Precipitation. Catalysts, 2019, 9, 524.	3.5	9
170	Kinetic modeling for direct synthesis of dimethyl ether from syngas over a hybrid Cu/ZnO/Al2O3/ferrierite catalyst. Catalysis Today, 2022, 388-389, 323-328.	4.4	9
171	Singleâ€Atom Catalysts: Synthesis Strategies, Catalytic Applications, and Performance Regulation of Singleâ€Atom Catalysts (Adv. Funct. Mater. 12/2021). Advanced Functional Materials, 2021, 31, 2170081.	14.9	9
172	CO2 Reforming of CH4 Using Coke Oven Gas over Ni/MgO-Al2O3 Catalysts: Effect of the MgO:Al2O3 Ratio. Catalysts, 2021, 11, 1468.	3.5	9
173	Catalytically stable monodispersed multi-core Ni-Co nanoparticles encapsulated with SiO2 shells for dry reforming of CH4 with CO2. Journal of CO2 Utilization, 2022, 60, 101984.	6.8	9
174	Comparison of normal and reverse precipitation methods in the preparation of Cu/ZnO/Al2O3 catalysts for hydrogenolysis of butyl butyrate. Catalysis Communications, 2014, 54, 1-5.	3.3	8
175	Dehydrochlorination of polyvinylchloride using Al-modified graphitic-C <sub>3</sub> N <sub>4</sub> . RSC Advances, 2016, 6, 20728-20733.	3.6	8
176	Effect of Mn promoter on Rh/tungsten carbide on product distributions of alcohols and hydrocarbons by CO hydrogenation. RSC Advances, 2016, 6, 101535-101543.	3.6	8
177	Horizontal immersed heater-to-bed heat transfer with layer inversion in gas-liquid-solid fluidized beds of binary solids. Chemical Engineering Science, 2017, 170, 501-507.	3.8	8
178	Effects of self-reduction of Co nanoparticles on mesoporous graphitic carbon-nitride to CO hydrogenation activity to hydrocarbons. Fuel, 2021, 287, 119437.	6.4	8
179	Facile Structure Tuning of a Methanol ynthesis Catalyst towards the Direct Synthesis of Dimethyl Ether from Syngas. ChemCatChem, 2017, 9, 4484-4489.	3.7	8
180	Thermo-catalytic decomposition of propane over carbon black in a fluidized bed for hydrogen production. International Journal of Hydrogen Energy, 2014, 39, 14800-14807.	7.1	7

#	Article	IF	CITATIONS
181	Tungsten oxides supported on nano-size zirconia for cyclic production of syngas and hydrogen by redox operations. Korean Journal of Chemical Engineering, 2014, 31, 961-971.	2.7	7
182	Removal of Benzoic Acid in Heavy Oils by Esterification Using Modified Ferrierite: Roles of BrÃ,nsted and Lewis Acid Sites. Energy & Fuels, 2016, 30, 5391-5397.	5.1	7
183	Direct synthesis of liquid fuels and aromatics from syngas over mesoporous FeZrOx catalyst mixed with Mo/ferrierite. Fuel, 2020, 264, 116851.	6.4	6
184	Development of dimethyl ether synthesis processes using by-product gas from a steel-making plant: Single-vs. two-step processes. Journal of Cleaner Production, 2021, 326, 129367.	9.3	6
185	A Novel Method of CCl4Disposal by Disproportionation with CH4over Pt on Various Supports. Chemistry Letters, 2001, 30, 264-265.	1.3	5
186	Disposal of CCl4 by Disproportionation Reaction with CH4. Industrial & Engineering Chemistry Research, 2007, 46, 7057-7065.	3.7	5
187	Effect of pressure fluctuations on the heat transfer characteristics in a pressurized slurry bubble column. Korean Journal of Chemical Engineering, 2008, 25, 897-904.	2.7	5
188	Effects of Reaction Variables on Fischer–Tropsch Synthesis with Co-Precipitated K/FeCuAlO x Catalysts. Catalysis Letters, 2011, 141, 799-807.	2.6	5
189	Differences in DNA Probe-Mediated Aggregation Behavior of Gold Nanomaterials Based on Their Geometric Appearance. Langmuir, 2018, 34, 14869-14874.	3.5	5
190	Adjusting Hydrocarbon Distribution on the Stabilized Alâ€Modified Mesoporous Co <sub>3</sub> O <sub>4</sub> â€Fe <sub>2</sub> O <sub>3</sub> Bimetal Oxides for CO Hydrogenation. ChemCatChem, 2020, 12, 2304-2314.	3.7	5
191	Contributions of post-synthesized mesopore structures of ferrierite zeolite for gas-phase dimethyl ether carbonylation activity. Korean Journal of Chemical Engineering, 2021, 38, 1231-1239.	2.7	5
192	Effect of distributor type on microbubble dispersion in a pressurized bubble column. Chemical Engineering Research and Design, 2021, 174, 188-198.	5.6	5
193	Carbonylation of Dimethyl Ether to Methyl Acetate on Zr-Modified Ferrierite. Advanced Porous Materials, 2016, 4, 200-205.	0.3	5
194	A superhydrophobic layer formed by fluoro-derivative-treated gold sheets on grown-up zinc oxide nanoparticles for a spherical DNA hydrogel. Colloids and Surfaces B: Biointerfaces, 2013, 111, 342-345.	5.0	4
195	Redox of titanium oxides by methane and water for application to cyclic syngas and hydrogen production systems. International Journal of Hydrogen Energy, 2015, 40, 2518-2528.	7.1	4
196	Nickel oxide-silica core-shell catalyst for acetylene hydroxycarbonylation. Catalysis Communications, 2019, 123, 86-90.	3.3	4
197	Thermo-catalytic decomposition of waste lubricating oil over carbon catalyst. Korean Journal of Chemical Engineering, 2016, 33, 2891-2897.	2.7	3
198	Catalytic Decomposition of Pyrolysis Fuel Oil over in Situ Carbon-Coated Ferrierite Zeolite for Selective Hydrogen Production. Energy & Fuels, 2018, 32, 3792-3799.	5.1	3

#	Article	IF	CITATIONS
199	Dehydrogenation of ethane and subsequent activation of CO2 on hierarchically-structured bimetallic FeM@ZSM-5 (M=Ce, Ga, and Sn). Korean Journal of Chemical Engineering, 2021, 38, 1129-1138.	2.7	3
200	Contributions of acidic-basic sites on hybridized FER@g-C3N4 for liquid-phase decarboxylation of naphthenic acids. Fuel, 2021, 296, 120679.	6.4	3
201	Effect of Heat Treatment on the Electrochemical Properties of Mn Oxide-Based Powder Prepared Using a Wet Chemical Process. Science of Advanced Materials, 2016, 8, 89-95.	0.7	3
202	Promoting Effect of Admixed Ce <sub>x</sub> Zr <sub>1-x</sub> O <sub>2</sub> with Cu-ZnO-Al <sub>2</sub> O <sub>3</sub> Methanol Synthesis Catalyst on Catalytic Performance: Influence of Ce/Zr Ratio. Bulletin of the Korean Chemical Society, 2010, 31, 470-472.	1.9	3
203	Dimethyl ether conversion to hydrocarbons on the closely interconnected FER@ZSM-5 nanostructures. Microporous and Mesoporous Materials, 2022, 340, 112034.	4.4	3
204	Nanosized seed-derived ferrierite zeolite for a gas-phase carbonylation of dimethyl ether to methyl acetate. Catalysis Today, 2022, , .	4.4	3
205	Liquid-phase Hydrodechlorination of CCl4with Co-production of Diethylcarbonate and Acetal. Chemistry Letters, 2002, 31, 1020-1021.	1.3	2
206	Methane reforming and water splitting by zirconia-supported cerium-tungsten composite oxides for cyclic production of syngas and hydrogen. International Journal of Hydrogen Energy, 2016, 41, 6220-6229.	7.1	2
207	Stable Syngas Production by Concurrent Methane Decomposition and Carbon Dioxide Gasification with Activated Carbon. Science of Advanced Materials, 2016, 8, 205-211.	0.7	2
208	Mechanistic kinetic modeling for catalytic conversion of DME to gasoline-range hydrocarbons over nanostructured ZSM-5. Catalysis Science and Technology, 2022, 12, 4798-4810.	4.1	2
209	Entrainment of Geldart C particles in fluidized beds with binary particles. Korean Journal of Chemical Engineering, 2014, 31, 2094-2100.	2.7	1
210	Modified Kinetic Model for Dichloropropanol Synthesis from Glycerin and Anhydrous HCl at High Pressure. Journal of Chemical Engineering of Japan, 2011, 44, 336-344.	0.6	1
211	Phosphorus Modified Co/Al <sub>2</sub> O <sub>3</sub> Fischer-Tropsch Catalyst for a Slurry Phase CSTR with Enhanced Hydrothermal and Mechanical Stability. Korean Chemical Engineering Research, 2012, 50, 229-237.	0.2	1
212	Fast Pyrolysis of Biomasses in a Bubbling Fluidized Bed Reactor. Journal of Chemical Engineering of Japan, 2012, 45, 862-867.	0.6	1
213	Modified Nano-Perovskite Catalysts for the Steam and CO <sub>2</sub> Reforming of Methane. Journal of Nanoscience and Nanotechnology, 2015, 15, 5889-5892.	0.9	0
214	Graphene: Microtopographyâ€Guided Conductive Patterns of Liquidâ€Driven Graphene Nanoplatelet Networks for Stretchable and Skinâ€Conformal Sensor Array (Adv. Mater. 21/2017). Advanced Materials, 2017, 29, .	21.0	0